

Detection of new O-type stars in the obscured stellar cluster Tr 16-SE in the Carina Nebula with KMOS [★]

T. Preibisch¹, S. Fleischlen¹, C. Göppl¹, B. Ercolano¹, and V. Roccatagliata^{2,3,4}

¹ Universitäts-Sternwarte München, Ludwig-Maximilians-Universität, Scheinerstr. 1, 81679 München, Germany
e-mail: preibisch@usm.uni-muenchen.de

² Dipartimento di Fisica “E. Fermi”, Università di Pisa Largo Bruno Pontecorvo 3, 56127 Pisa, Italy

³ INAF-Osservatorio Astrofisico di Arcetri, Largo E. Fermi 5, 50125 Firenze, Italy

⁴ INFN, Sezione di Pisa, Largo Bruno Pontecorvo 3, 56127 Pisa, Italy

Received 7 October 2020; accepted 11 February 2021

ABSTRACT

Context. The Carina Nebula harbors a large population of high-mass stars, including at least 75 O-type and Wolf-Rayet (WR) stars, but the current census is not complete since further high-mass stars may be hidden in or behind the dense dark clouds that pervade the association.

Aims. With the aim of identifying optically obscured O- and early B-type stars in the Carina Nebula, we performed the first infrared spectroscopic study of stars in the optically obscured stellar cluster Tr 16-SE, located behind a dark dust lane south of η Car.

Methods. We used the integral-field spectrograph KMOS at the ESO VLT to obtain *H*- and *K*-band spectra with a resolution of $R \approx 4000$ ($\Delta\lambda \approx 5\text{\AA}$) for 45 out of the 47 possible OB candidate stars in Tr 16-SE, and we derived spectral types for these stars.

Results. We find 15 stars in Tr 16-SE with spectral types between O5 and B2 (i.e., high-mass stars with $M \geq 8 M_{\odot}$), only two of which were known before. An additional nine stars are classified as (Ae)Be stars (i.e., intermediate-mass pre-main-sequence stars), and most of the remaining targets show clear signatures of being late-type stars and are thus most likely foreground stars or background giants unrelated to the Carina Nebula. Our estimates of the stellar luminosities suggest that nine of the 15 O- and early B-type stars are members of Tr 16-SE, whereas the other six seem to be background objects.

Conclusions. Our study increases the number of spectroscopically identified high-mass stars ($M \geq 8 M_{\odot}$) in Tr 16-SE from two to nine and shows that Tr 16-SE is one of the larger clusters in the Carina Nebula. Our identification of three new stars with spectral types between O5 and O7 and four new stars with spectral types O9 to B1 significantly increases the number of spectroscopically identified O-type stars in the Carina Nebula.

Key words. Stars: formation – Stars: pre-main sequence – open clusters and associations: Tr 16-SE – stars: O/B classification

1. Introduction

The Carina Nebula, at a distance of ≈ 2.3 kpc (see Smith & Brooks 2008, for a review), is one of the most massive and active star forming regions in our Galaxy and harbors a large population of high-mass stars ($M \geq 8 M_{\odot}$). With 70 optically identified O-type stars, three known Wolf-Rayet (WR) stars, and η Car with its companion (see Smith 2006; Alexander et al. 2016; Hanes et al. 2018), the currently known population comprises 75 stars with masses above $18 M_{\odot}$. These massive stars constitute a large OB association, in which Tr 14, 15, and 16 are the most prominent open clusters in optical images.

The Carina Nebula still contains a very large mass ($\sim 10^6 M_{\odot}$; Preibisch et al. 2012) of dusty gas clouds. Maps of the cloud column density derived from far-infrared (Preibisch et al. 2012), submillimeter (Preibisch et al. 2011c), and CO observations (Rebolledo et al. 2016) show that the structure of these clouds is very inhomogeneous and that the visual cloud extinction reaches values of $A_V \sim 10$ mag or more at several locations in the nebula. Given the considerable obscuration effect of these dark clouds, only deep infrared observations can reveal the full stellar population. Deep near-infrared (NIR) sur-

veys of the Carina Nebula have been obtained with HAWK-I on the Very Large Telescope (VLT) at the European Southern Observatory (ESO; Preibisch et al. 2011b) as well as with the VISTA telescope (Preibisch et al. 2014). The Carina Nebula was also mapped at mid-infrared wavelengths with the *Spitzer* Space Observatory (Smith et al. 2010). In combination with the comprehensive X-ray observations obtained in the *Chandra Carina Complex Project* (CCCP; see Townsley et al. 2011), these infrared data yielded comprehensive information about the stellar populations (e.g., Feigelson et al. 2011; Preibisch et al. 2011a; Povich et al. 2011).

However, the current census of high-mass stars in the Carina Nebula is probably still substantially incomplete. For example, Roccatagliata et al. (2013) found that the total far-infrared luminosity of the cloud complex is $\approx 70\%$ larger than expected from the total stellar far-ultraviolet luminosity of the currently known OB stars. The analysis of bright *Spitzer* infrared sources by Povich et al. (2011) led to the identification of 94 new candidate OB stars in the Carina Nebula with extinction values up to $A_V \approx 35$ mag.

Due to the location of the Carina Nebula very close to the galactic plane, the vast majority of all detected infrared sources are distant field stars in the galactic background. The only way to reliably identify obscured OB stars among the many background

[★] Based on observations collected at the European Southern Observatory under ESO program 097.C-0102.

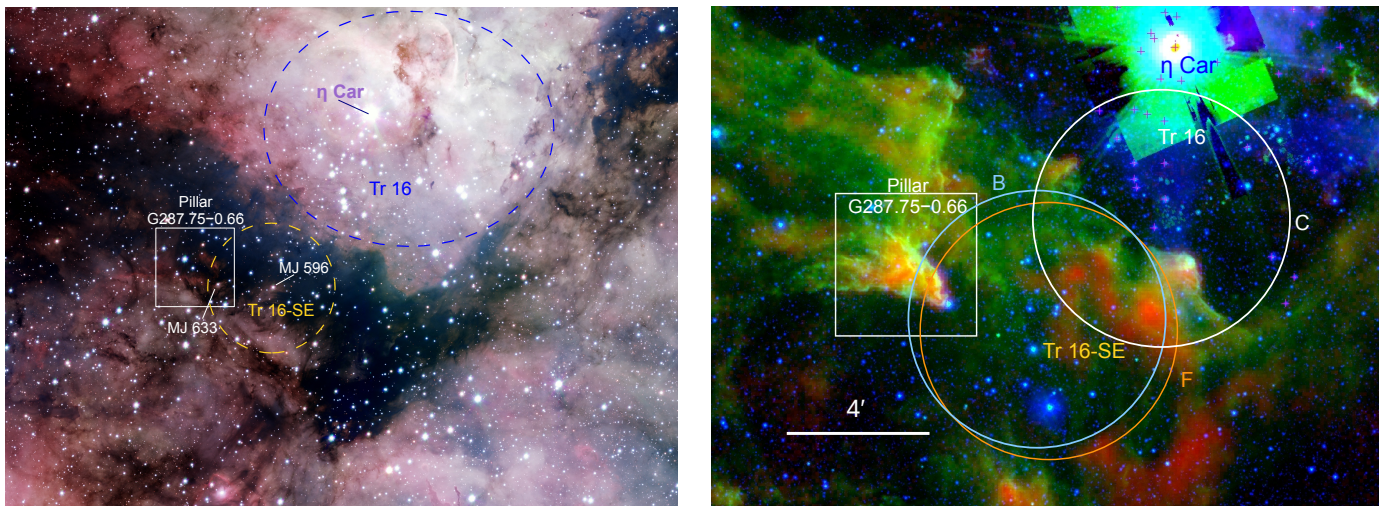


Fig. 1. Optical and infrared images of the central part of the Carina Nebula. Left: Optical image reproduced from the ESO Photo Release eso1250 (image credit: VPHAS+ Consortium/Cambridge Astronomical Survey Unit). It is composed of a *B*-band image in the blue color channel, a *g*-band image in the green color channel, and *r*-band and *H α* -band images in the red color channel. The white box marks the region around the pillar G 287.75–0.66 (which is not visible in this optical image). The dashed yellow circle marks the region of the obscured cluster Tr 16-SE and the dashed blue ellipse the cluster Tr 16. The positions of the stars MJ 596, MJ 633, and η Car are marked. North is up, and east is to the left. Right: Color composite image of the region around the pillar, composed from our VISTA *K_s*-band image in blue, the *Spitzer* 5.8 μ m image in green (where the area around η Car [near the upper right corner] is affected by saturation), and our LABOCA 870 μ m map in red. The white 4' \times 4' square marks the region of the pillar G 287.75–0.66, and the circles show the KMOS patrol fields for the **B** (blue), **F** (orange), and **C** (white) observations. North is up, and east is to the left.

contaminators is thus by spectroscopy. Spectroscopic surveys (see the summary in Smith 2006, for earlier observations) have, however, so far only been performed for the unobscured population of optically bright stars (Alexander et al. 2016; Damiani et al. 2017; Mohr-Smith et al. 2017; Kiminki & Smith 2018). This lack of spectroscopic information for the obscured, optically faint high-mass star candidates is a serious gap in our knowledge of the stellar population in the Carina Nebula and limits our understanding of the global energetics and feedback processes in this important star forming region.

The V-shaped dark cloud structure that intersects the central parts of the Carina Nebula contains a clustering of infrared and X-ray sources, denoted as Tr 16-SE (Sanchawala et al. 2007; Smith et al. 2010; Feigelson et al. 2011), about 9 arcminutes southeast of η Car and the optically prominent stellar cluster Tr 16 (see Fig. 1). Most stars in Tr 16-SE are invisible or very faint in optical images, and until recently the only star with a known optical spectral type was the double-lined O5.5V+O9.5V spectroscopic binary MJ 596 (Niemela et al. 2006), also known as V662 Car. The study of the bright *Spitzer* point sources by Povich et al. (2011) found six candidate OB stars in Tr 16-SE, but none of these have been confirmed with spectroscopy to date. This makes Tr 16-SE a very interesting target for the search for still unidentified high-mass stars in the Carina Nebula.

The very high levels of ionizing radiation and stellar wind power from the numerous massive stars in the Carina Nebula profoundly influence the surrounding clouds, making it a textbook example for studies of stellar feedback and the resulting processes of cloud disruption and triggered star formation. The infrared to submillimeter images (see Smith et al. 2010; Preibisch et al. 2012, 2011c) revealed numerous pillar-like cloud structures in the southern parts of the Carina Nebula. Such pillars are thought to be a natural outcome of the feedback from strong ionizing radiation fields on clouds (see, e.g., Gritschneider et al. 2010; Dale et al. 2013; McLeod et al. 2016; Klaassen et al.

2020). While almost all pillars in the Carina Nebula point toward the massive stars around η Car in Tr 16, the *Spitzer* image (see Fig. 1) reveals one prominent exception approximately 9' southeast of η Car, where one bright and well-structured pillar does not point toward η Car (which would be north) but instead points in a southwestern direction toward a region where no particularly bright stars are seen in optical images. This pillar was denoted as G 287.75–0.66 by Smith et al. (2010) and is part of the cloud structure that creates the remarkable V-shaped dark lane in the central part of the Carina Nebula in optical images (see Fig. 1). Interestingly, this pillar only points in the direction of the obscured cluster Tr 16-SE.

Our aims are thus to perform the first systematic spectroscopic study of the stellar population in Tr 16-SE and thus improve the census of massive stars ($M \geq 8 M_{\odot}$) in the Carina Nebula; we are therefore interested in identifying stars with spectral types from O to B2, which we call “OB2 stars” in the following. Due to the high level of obscuration, most stars in Tr 16-SE are too faint for optical spectroscopy; we therefore obtained NIR spectra for a magnitude-limited sample of 50 stars in the cluster.

2. K-band Multi-Object Spectrograph observations

2.1. Target sample and observing strategy

Our goal was to obtain *H*- and *K*-band infrared spectra of all potential high-mass stars in Tr 16-SE ($M \gtrsim 8 M_{\odot}$, corresponding to spectral types from O to B2) in the Carina Nebula. The target stars were selected from our VISTA photometry catalog of the Carina Nebula (see Preibisch et al. 2014). A brightness limit of $K_s \leq 12$ mag was chosen because any star at the distance of the Carina Nebula with a mass of $M \geq 8 M_{\odot}$ [$M \geq 18 M_{\odot}$] will be brighter than this limit for extinctions of up to $A_V \approx 11$ mag [$A_V \approx 28$ mag]. We can thus be confident that such a magnitude-limited sample will contain all the O-type stars ($M \geq 18 M_{\odot}$) and most of the early B-type stars ($8 M_{\odot} \leq M \leq 18 M_{\odot}$) in Tr 16-SE.

We did not use any further conditions (e.g., luminosity estimates from spectral energy distribution analysis or X-ray detection) in the construction of our sample in order to keep it as unbiased as possible.

As the spatial selection region for our Tr 16-SE sample, we used a $5.7' \times 5'$ box centered at the J2000 coordinates R.A. = $10^{\text{h}} 45^{\text{m}} 31.7^{\text{s}}$ and Dec = $-59^{\circ} 48' 48''$. This area contains 47 stars¹ with $K_s \leq 12$. We were able to obtain spectra of 45 of these 47 stars (i.e., we have an observational completeness of 95.74%); the only two stars in our selection region that could not be observed are VCNS J104554.89-594818.8 ($K_s = 7.84$) and VCNS J104554.36-595006.6 ($K_s = 11.75$).

Due to the number of our targets and the wide range of magnitudes of the individual target stars, the observational sequence was split into three individual observations, denoted as the **B** (bright star), **F** (faint star), and **C** (calibrator star) observations in the following. The **B** observation contained the stars in Tr 16-SE with $K_s \approx [7.0 - 10.6]$ mag and $H \approx [7.5 - 11.7]$ mag. The **F** observation contained the stars in Tr 16-SE with $K_s \approx [10.6 - 12.0]$ mag and $H \approx [10.8 - 13.2]$ mag.

The **C** observation targeted 14 known high-mass stars in the cluster Tr 16, for which spectral types between O5 and B2 had been previously determined from optical spectroscopy; Table 1 lists the positions, names, and spectral types of these stars. They were observed and analyzed in the same way as our target stars in Tr 16-SE and then used as spectral standards for the classification of the target stars in Tr 16-SE. Figure 1 shows the positions of the three observations.

2.2. KMOS configuration

The *K-band Multi-Object Spectrograph* (KMOS) at the ESO VLT allows the simultaneous observation of up to 24 target stars within a circular $7.2'$ diameter patrol field. As described in more detail in Sharples et al. (2013) and on the ESO instrument web page², KMOS employs 24 configurable arms that position pick-off mirrors at user-specified locations in the focal plane. Each subfield is fed to an image slicer integral-field unit (IFU) with a square field of view of $2.8'' \times 2.8''$ that provides a uniform spatial sampling of $0.2'' \times 0.2''$. The light from each IFU is then dispersed by grating spectrometers that generate 14×14 spectra with ~ 1000 Nyquist-sampled spectral resolution elements.

While KMOS allows a rather flexible spatial placement of the 24 individual pickoff mirrors, there are some restrictions on the configuration, for example, a minimum distance of at least $6''$ between two neighboring pickoff mirrors. It is thus not always possible to observe all desired target stars in one field. After performing detailed experiments, we were finally able to establish configurations for the three observations that allowed us to obtain spectra of 45 out of the 47 OB candidate stars in Tr 16-SE and all 14 calibrator stars.

The resulting spectra are denoted by the corresponding **B**, **F**, or **C** prefixes and a running number corresponding to the IFU (e.g., B1). While the target stars were generally centered on the IFU, our target star, J104530.29-594824.5, has a close companion (J104530.42-594825.4, angular separation $1.3''$), and as such both stars could be observed in one IFU (F12); their spectra are denoted as F12-1 and F12-2. In order to employ all avail-

able KMOS arms in the **F** observation, we also observed one star (F21) with $K_s = 12.24$, which is slightly fainter than our magnitude limit.

Since the **C** observation partly overlapped with the Tr 16-SE target field (see Fig. 1), six of the KMOS arms not needed for the calibrator stars were used for additional, redundant observations of target stars in Tr 16-SE; the two spectra of these double observations were reduced and analyzed independently, and they served as a consistency check for our analysis. Furthermore, three KMOS arms (C16, C17, and C18) were put on stars in or near the cluster Tr 16.

In each observation, one KMOS arm was used for a simultaneous sky observation. The coordinates of the stars in our three different observations (**B**, **F**, and **C**) are listed in Table 3.

2.3. Spectroscopic observations

We obtained KMOS spectra in the *H* and the *K* spectral bands, which provide a wavelength coverage of $[1.456 - 1.846] \mu\text{m}$ and $[1.934 - 2.460] \mu\text{m}$, respectively, and a spectral resolving power of $R(H) \approx 4040$ and $R(K) \approx 4230$. The observations were carried out on 21 February 2016 (PI: Preibisch, 097.C-0102(A)) between 02:37:34 UT and 04:58:25 UT under photometric sky conditions. The median Differential Image Motion Monitor (DIMM) seeing at 500 nm was $\approx 1.4''$; the corresponding full width at half maximum (FWHM) of the point spread function (PSF) in the NIR is $\approx 1.0''$. For each observation, target and sky-offset exposures were alternated in a target-sky-target sequence. The sky regions were observed by rotating and shifting the arms without altering the configuration. Each science observation was performed with three dither positions and a dither size of $0.2''$.

For the **B** and **C** observations, the individual integration time was 3 seconds and the number of integrations was 14 (13) for the *H*-band (*K*-band), resulting in a total exposure time of 42 s (39 s). Furthermore, an additional long exposure on sky of 42 (39) seconds for the *H*-band (*K*-band) was executed at the end of each science observation. For the **F** observation, the individual integration time was 20 seconds; the number of integrations was eight (six) for the *H*-band (*K*-band), leading to a total exposure time of 160 s (120 s).

2.4. Data reduction

The data were reduced using the ESO Recipe Flexible Execution Workbench (Reflex) and the ESO Recipe Execution Tool (esorex), as described by (Freudling et al. 2013), using the standard KMOS/esorex routines. Sky subtraction and telluric correction were performed with the sky tweaking method described by Davies et al. (2013b); a comprehensive description of the method can be found in Coccatto et al. (2019). The standard star used for the telluric correction (and later also for flux calibration) was the B3V star HD 93695.

From the final data cubes, spectra were extracted using the “optimal extraction method” provided by the pipeline. For the two cases where more than one source was present per IFU (targets F12-1 & F12-2 and targets B24 & F24), the extraction was performed manually with QFitsViewer, employing circular apertures with radii of 2 pixels and 3 pixels.

¹ We excluded the star BM VII 10 (= 2MASS J10453185-5951094) because it is known to be an S star (see Van Eck et al. 2000), i.e., a cool giant, and would have been much too bright ($K_s = 5.0$) for our observations.

² <https://www.eso.org/sci/facilities/paranal/instruments/kmos.html>

Table 1. Calibrator star sample.

KMOS spectrum	J2000 coordinates [hh:mm:ss.ss–dd:mm:ss.s]	Star Name	Spectral type	
			[Smith]	[Sota]
C2	10:44:41.76–59:46:56.3	CPD-59 2600	O6 V((f))	O6 V((f))
C3	10:44:47.29–59:43:53.2	CPD-59 2603A	O7 V((f))	O7.5 V
C4	10:45:12.71–59:44:46.0	CPD-59 2635A	O8 V	O8 V
C5	10:45:12.87–59:44:19.2	CPD-59 2636A	O7 V	O8 V
C6	10:45:16.51–59:43:37.0	CPD-59 2641	O5 V	O6 V
C7	10:45:12.21–59:45:00.3	HD 93343	O7 V(n)	O8 V
C8	10:45:05.84–59:43:07.7	Tr 16-9	O9.5 V	O9.7 IV
C9	10:45:08.22–59:46:06.9	Tr 16-22	O8.5 V	O8.5 V
C10	10:45:05.79–59:45:19.5	Tr 16-23	O7 V	O7.5 V
C11	10:45:05.87–59:44:18.8	Tr 16-24	B2 V	–
C12	10:45:09.74–59:42:57.2	Tr 16-74	B1 V	–
C13	10:45:12.65–59:42:48.7	Tr 16-76	B2 V	–
C14	10:45:20.57–59:42:51.2	Tr 16-115	O8.5 V	O9 V
C15	10:44:59.90–59:43:14.9	CPD-59 2618	B1.5 V	

Notes. The spectral types listed in Col. 4 are from Smith (2006), and those in Col. 5 are from Sota et al. (2014); the spectral type of CPD-59 2618 is from Massey & Johnson (1993).

Table 2. Parameters of the KMOS observations.

Observation	Aimpoint (J2000)	Obtained Spectra	Exposure Time
B	10:45:35.0 –59:48:45	23 target stars	14 × 3 s = 42 s (H), 13 × 3 s = 39 s (K)
F	10:45:31.7 –59:49:07	24 target stars	8 × 20 s = 160 s (H), 6 × 20 s = 120 s (K)
C	10:45:07.6 –59:45:52	14 spectral calibrators + 9 target stars	14 × 3 s = 42 s (H), 13 × 3 s = 39 s (K)

2.5. Resulting spectra

The resulting spectra were flux-calibrated using the B3V standard star and stored in units of $\text{erg s}^{-1} \text{cm}^{-2} \text{\AA}^{-1}$. They have a spectral dispersion of 2.16 \AA per pixel in the *H*-band and 2.81 \AA per pixel in the *K*-band. For the analysis of the line strengths, we performed a continuum normalization of all spectra with cubic spline interpolation using ten to 30 points in the continuum. The normalized spectra are displayed in Figs. A.1 to A.6.

In order to characterize the quality of our spectra, we determined the signal-to-noise ratio (S/N) with the DER_SNR algorithm described in Stoehr et al. (2008). In order to avoid spectral regions with strong features, we used the wavelength intervals $[1.62 - 1.63] + [1.65 - 1.67] \mu\text{m}$ for the *H*-band and $[2.12 - 2.15] + [2.22 - 2.25] \mu\text{m}$ for the *K*-band. The S/N of the target spectra ranges from values of 14 to 545 with a mean (median) value of 132 (81) for the *H*-band, and from values of 26 to 348 with a mean (median) value of 115 (95) for the *K*-band.

3. Spectral classification

3.1. Classification strategy

Since the aim of our study was to identify high-mass stars ($M \geq 8 M_{\odot}$) in the Carina Nebula, we focused our efforts on those targets that show evidence of being of O- or early B-type stars (not later than B2), which we denote as OB2 stars. The primary spectral indicators for these hot stars are the helium lines. It is well established (see, e.g., Gray & Corbally 2009; Hanson et al. 2005) that stars with spectral types earlier than B3 generally show He I lines and that stars with spectral types O8 or earlier also show He II lines. These expectations are very well confirmed in the spectra of our calibration stars that have optically determined spectral types. We therefore considered all stars

that clearly show He lines as OB2 stars and estimated their spectral types as described in Sect. 3.3.

Stars that show no clear He lines must have spectral types later than B2 and thus stellar masses $< 8 M_{\odot}$. As these stars are not relevant for the aims of our study and because our target sample is clearly incomplete in this mass range, we limited our efforts to characterizing such stars with crude estimates. The $K_s \leq 12$ mag limit for our target sample implies the lower limit in stellar mass (or spectral type) that we can expect to find in our sample if the target star is at the distance of the Carina Nebula. According to the CMD 3.3 web interface³ for the PARSEC stellar models (Bressan et al. 2012), this magnitude limit corresponds to a stellar mass of $\sim 2.5 M_{\odot}$ and a late F to early G spectral type for stars at ages between 1 and 3 Myr if there is no extinction. We thus expect that our sample should contain some intermediate-mass young stars, some of which should display the typical spectral signature of Herbig AeBe stars (see Herbig 1994).

These considerations also imply that any cool stars (spectral type later than G) we find in our sample must either be foreground stars or red giants; in both cases, these stars would be unrelated “field stars” (since no red giants are expected to be present in the young stellar population of the Carina Nebula). Therefore, stars with cool spectra are not interesting⁴ for the purposes of our study.

3.2. Diagnostic lines in the KMOS spectra

For the classification of our target stars we used the following diagnostic lines in the *H*- and *K*-bands.

³ <http://stev.oapd.inaf.it/cgi-bin/cmd>

⁴ The possibility of RSG stars (i.e., evolved massive stars) will be addressed in Sect. 3.4.

3.2.1. He II lines

Our KMOS spectra contain the He II 7–12 line at $1.6918\ \mu\text{m}$ and the He II 7–10 line at $2.1885\ \mu\text{m}$, both of which are clear signatures of O-type stars. In our calibrator sample, the He II 7–12 line is clearly present in all stars down to spectral type O6 but is not seen in later type stars; it shows equivalent widths up to $0.35\ \text{\AA}$ in the hottest stars. The He II 7–10 line is clearly seen in the hottest stars and down to spectral type O7.5, but not in later type stars; it shows equivalent widths up to $1.0\ \text{\AA}$ in the hottest stars.

3.2.2. He I lines

For our analysis, we used the He I $1s3p\ ^3P^0 \rightarrow 1s4d\ ^3D$ triplet at $1.7002\ \mu\text{m}$, the He I $1s3p\ ^3P^0 \rightarrow 1s4s\ ^3S$ triplet at $2.1120\ \mu\text{m}$, and the He I $1s3p\ ^3P^0 \rightarrow 1s4s\ ^1S$ line and $2.1132\ \mu\text{m}$, the second and third of which form a blend at $\approx 2.1126\ \mu\text{m}$ at the resolution of our KMOS spectra. In our calibrator sample, these He I lines are seen in all O-type stars and down to spectral type B2 (the latest spectral type in our calibrator sample). The strength of He I $1.7002\ \mu\text{m}$ increases from $0.5\ \text{\AA}$ for the O5 stars toward $1.9\ \text{\AA}$ in the early B-type stars. The He I $2.1126\ \mu\text{m}$ line shows a similar tendency of line strength versus spectral type, but it appears in emission (with equivalent widths up to $-3\ \text{\AA}$) in the hottest (O5) stars. It is blue-shifted in the stars later than O6. These He I lines are expected to disappear in stars cooler than spectral types B3–4 (see, e.g., Repolust et al. 2005).

3.2.3. H lines

Our spectra contain the Br 7 ($2.1655\ \mu\text{m}$) to Br 15 ($1.5701\ \mu\text{m}$) atomic hydrogen lines. Most of these, in particular the Br 7 (= Bry) line, are seen in all our calibrator spectra. As expected, their line strength generally decreases with increasing temperature. The equivalent widths of the Bry line in our calibrator spectra range up to $6.5\ \text{\AA}$; the line is seen in emission in one star. In general, strong Bry lines are also seen in substantially cooler (late B, A, and F) stars and are expected to disappear only at late G spectral types.

3.2.4. Na I and Ca I lines

The Na I lines at $2.2056\ \mu\text{m}$ and $2.2084\ \mu\text{m}$ and the Ca I lines at $2.2608\ \mu\text{m} + 2.0796\ \mu\text{m} + 2.0836\ \mu\text{m}$ are clear signatures of cool stars (spectral type G or later). They are generally absent in the spectra of our OB2 calibrator stars. We note that one of our calibrator stars shows the $2.2056\ \mu\text{m}$ Na I line in absorption, but this line is very narrow (much less broad than the other lines), suggesting an interstellar origin for the absorption.

3.2.5. CO band heads

The CO ro-vibrational bands, with their band heads at $2.2935\ \mu\text{m}$ for the $\nu = 2 - 0$ transitions, $2.3227\ \mu\text{m}$ for the $\nu = 3 - 1$ transitions, and $2.3535\ \mu\text{m}$ for the $\nu = 4 - 2$ transitions, constitute very prominent absorption features in cool stars. They are generally seen at spectral types later than mid G. None of our OB2 calibrator spectra show these band heads.

3.3. Spectral type determination for the O- and early B-type stars

Spectral classification of early-type stars in the infrared regime is less reliable than in the optical (see Gray & Corbally 2009), mostly because the lines in the NIR regime are often formed in higher atmospheric layers than the optical lines. In particular, the equivalent width of the H and He lines in hot stars not only depends on the effective temperature, but is also strongly influenced by the surface gravity and the detailed properties of the (generally very strong) stellar winds (see, e.g., Hanson et al. 2005; Repolust et al. 2005). Nevertheless, the He lines show a systematic increase or decrease in line strength with spectral type, which allows spectral types to be reasonably well determined.

The general trends of decreasing line strengths with increasing temperature for the H and He I lines and the increasing line strengths with increasing temperature for the He II lines are clearly seen in the spectra of our calibrator stars, although with a substantial scatter. Given the moderate spectral resolution of our spectra and the limited number of just four diagnostic He lines we can use, we do not aim at a very detailed and highly accurate spectra modeling but instead restrict our analysis to estimating spectral types with an accuracy of about two subtypes.

For all the stars in our samples that showed clear He lines, we analyzed the strengths of the diagnostic lines described below to determine their spectral type as accurately as possible. In order to avoid biases in the classification procedure, we did our classification for all KMOS spectra (i.e., including those stars for which a spectral type was already known from the literature). For stars that were observed twice, the classification was also done twice. The analysis was also done in a “blind” way, that is, without taking the literature information into account. Only after finishing the classification did we check the corresponding literature values, and we compared our two independent spectral types for those stars that were observed twice. We generally found rather good agreement (within about two subtypes) in all cases.

3.4. Excluding the presence of Red Supergiants

As described above, we consider cool stars to be either foreground field stars or background giants, in any case unrelated to the Carina Nebula. However, a potential complication arises from the fact that some evolved massive stars spend a small fraction of time near the end of their lifetimes as red supergiants (RSGs) and display (very) cool spectra in this phase. Young stellar populations with ages of at least about 10 Myr can thus contain RSGs. Although it appears likely that the stars in Tr 16-SE are too young to be RSGs (the oldest age of the well-studied clusters in the Carina Nebula is 8 Myr [for Tr 15]; see Preibisch et al. (2011a)), this possibility should not be a priori excluded. Therefore, we checked whether the cool stars might possibly be RSGs in the Carina Nebula.

For this, we used the fact that RSGs generally have bolometric luminosities of $\gtrsim 10^4 L_{\odot}$ and employed the magnitude-luminosity calibration for RSGs derived by Davies et al. (2013a). Although the (unknown) extinction toward our target stars is a possible complication, it is not a very serious one for the purposes of our estimates for two reasons: First, we work in the infrared, and the extinction in the K-band is almost a factor of ten lower than in the optical. Second, from the color-color diagram of our target stars as well as from the cloud column density maps from our previous APEX/LABOCA submillimeter and *Herschel*

far-infrared maps, we know that the cloud extinction in TR 16-SE ranges from values of just a few magnitudes to about 15 magnitudes in optical extinction, corresponding to A_K values of $\lesssim 1.5$ mag. Since the minimal luminosity of RSGs is $\approx 10^4 L_\odot$, this implies that, even for an extinction of $A_V \approx 15$ mag, all possible RSGs should be brighter than $K \approx 5.7$. We note that this value is consistent with corresponding estimates based on the K -band bolometric corrections for cool stars from Buzzoni et al. (2010); thus, this magnitude limit is robust.

All our target stars have K -band magnitudes > 6.74 (and > 7.7 for all but the two brightest stars). We can therefore conclude that even the brightest stars in our sample are substantially fainter (by more than one magnitude in the K -band) than the expected magnitudes of even the faintest RSGs in the Carina Nebula. The cool stars in our sample must therefore be either foreground stars or giants (and perhaps RSGs) in the galactic background.

3.5. Results of the spectral classification

Our spectral typing results for each target star are listed in Table 3. The statistics as a function of spectral types are as follows.

Three stars are classified as "early O-type stars" ($\leq O5$): B8 (O5-6), B13 (O5), and B14 (O5). One of these, B13 = V662 Car = MJ 596, was known before our observation to be a double-lined O5.5V+O9.5V spectroscopic binary (Niemela et al. 2006) and was reclassified to a spectral type of O5Vz+B0:V by Alexander et al. (2016).

Three stars (B5, F3, and B7) are classified as "mid O-type stars" (O6 – O7). We note that for our target star, B5, an optically determined spectral type of O6 V became available in the literature (Alexander et al. 2016) after our KMOS observations.

One star (F8) is classified as a "late O-type star" (O8 – O9), five stars (F7, B12, B18, F22, and B21) as "late O- to early B-type stars" (O9 – B1), and three stars (F9, F16, and F17) as "early B-type stars" (B0 – B2). Eight stars (F10, F11, F12-2, B11, F14, B16, B17, and F21) are classified as "likely AeBe stars" (i.e., intermediate-mass pre-main-sequence stars).

The total combined number of OB2 and likely AeBe stars in the Tr 16-SE region is thus 23 (15 plus eight). We note that one of the three target stars outside Tr 16-SE, C17 in Tr 16, is also classified as a likely AeBe star.

The spectra of 18 stars in Tr 16-SE showed no indications of He lines but clear signatures of cool photospheres (e.g., CO absorption and/or Na and Ca line absorption), and are thus classified as cool stars. Six stars (F4, F12-1, F13, F15, B22, and B23) could not be reliably classified; some of them may be late B- or A-type stars.

4. Comparison to previous OB-candidate samples and photometric spectral type estimates

Povich et al. (2011) used photometry from 2MASS and *Spitzer* to analyze the spectral energy distributions (SEDs) of infrared sources in the Carina Nebula. In Tr 16-SE, they identified six stars (their OBc 48, 50, 51, 52, 56, and 61) as candidate OB stars based on their observed SED. All six of these stars are in our sample, and all of them are classified as O-type or early B-type stars in our independent spectroscopic analysis. This shows that the SED-based classification of OB candidate stars performed by Povich et al. (2011) worked very well and yielded reliable results.

In addition to the six OB candidates from Povich et al. (2011), our spectroscopic survey yields a further nine OB2 stars that were not in their OB-candidate sample. One of these is the previously known O5 star MJ 596, and our analysis (see below) suggests that six of these additional OB2 stars are background objects. However, two of these additional OB2 stars (B12 and B18, both classified as O9–B1 stars) are found to be members of Tr 16-SE. This shows that, as expected, the sample of SED-selected OB candidates from Povich et al. (2011) is not 100% complete; considering our results, the level of completeness is estimated to be $6/8 = 75\%$.

For several of our target stars, Mohr-Smith et al. (2017) reported spectral type estimates based on an analysis of their optical-infrared SED⁵ after our KMOS observations. We compared their spectral type estimate to our KMOS spectroscopic classifications and found generally rather good agreement, typically within one or two subtypes.

5. Clues on stellar distances from Gaia data

As mentioned in Sect. 2.1, our target stars were selected based only on their position on the sky and a limit on their K_s -band magnitude. Our target sample therefore contains not only stars in the Carina Nebula, but also some foreground and background stars. The Gaia mission (Gaia Collaboration et al. 2016) has recently determined parallax values for many of our target stars, providing very important distance information (which was not available at the time of our observations). We therefore checked whether we can use the Gaia data to identify foreground or background stars in our sample. This requires a good knowledge of the distance to the Carina Nebula and Tr 16-SE.

5.1. The distance to the Carina Nebula

As described in Smith & Brooks (2008), the pre-Gaia distance to the central region of the Carina Nebula is well known to be 2.3 kpc. Since the projected extent of the whole Carina Nebula cloud complex is about 100 pc (Preibisch et al. 2012, 2017), different parts of the complex may well be about 100 pc closer or more distant.

Although the Gaia data offer a good opportunity to investigate the distances in a new and independent way, the typical uncertainties of the Gaia Early Data Release 3 (EDR3) parallaxes and proper motions for most stars in the Carina Nebula are still too large to allow a purely astrometric identification of the Carina Nebula association members. One therefore needs a pre-selected sample of member candidates to determine distances with the Gaia data. Using the Gaia DR2 data, Povich et al. (2019) presented a determination of the distance to the large sample of $> 10\,000$ X-ray selected stars in the Carina Nebula from the CCCP project (see Broos et al. 2011) and found a value of $2.50^{+0.28}_{-0.23}$ kpc, slightly higher than but still consistent with the previous "canonical" value of 2.3 kpc.

Taking advantage of the recently released Gaia EDR3 data (see Gaia Collaboration et al. 2020), which provide improved accuracy of the astrometric parameters, we determined the mean value of the parallaxes of the 10 714 X-ray selected "likely Carina member stars" from the CCCP project; this yielded $\langle \varpi \rangle = 0.4347$ mas, corresponding to a distance of ≈ 2.30 kpc, in very good agreement with the pre-Gaia distance value.

⁵ We note that Mohr-Smith et al. (2017) also obtained optical spectra of some of their target stars, but none of these spectrally observed stars are located in the area of our TR 16-SE KMOS observations.

5.2. Gaia distances of the KMOS target stars

For 58 of the stars observed with KMOS, we could find a Gaia EDR3 match within a search radius of one arcsecond. For six stars, the listed parallaxes are negative (i.e., provide no useful information about the distance). The uncertainties of the Gaia parallaxes of our KMOS target stars range from $\sigma_{\varpi} = 0.0102$ mas up to $\sigma_{\varpi} = 0.5119$ mas.

Assuming that the stars in the Carina Nebula are in the distance range between ≈ 2.2 kpc and ≈ 2.8 kpc, we can check how consistent the parallax of individual KMOS target stars is with this distance range. For the large majority of our KMOS target stars, the $[\varpi \pm 3\sigma_{\varpi}]$ interval overlaps with the $[\frac{1}{2.8} - \frac{1}{2.2}]$ mas range; we consider the parallaxes of these stars as being consistent with membership in the Carina Nebula.

5.3. Foreground stars

We consider stars as "likely foreground stars" if their 3σ lower bound of the measured parallax is $\varpi - 3\sigma_{\varpi} > \frac{1}{2.2}$ mas, and as "clear foreground stars" if their 5σ lower bound of the measured parallax is $\varpi - 5\sigma_{\varpi} > \frac{1}{2.2}$ mas. According to these definitions, five of our target stars are clear foreground stars: B3=C21 ($1/\varpi = 1442$ pc), B4=C22 ($1/\varpi = 389$ pc), B22 ($1/\varpi = 486$ pc), B23 ($1/\varpi = 1398$ pc), and F24 ($1/\varpi = 1337$ pc). In addition, the two target stars C18 ($1/\varpi = 1991$ pc) and F23 ($1/\varpi = 1934$ pc) are likely foreground stars.

In our KMOS spectral classification, the Gaia-based foreground stars B3, F24, and C18 were classified as cool stars, B4 as a spectral type between F and G, and B22 and B23 as possible B- or A-type stars; these spectral types are consistent with their nature as field stars in the foreground. None of the OB2 stars in our KMOS sample have Gaia parallaxes that would suggest their being foreground stars.

5.4. Background stars

A similar attempt to identify possible background stars was not successful. Although a couple of stars have suspiciously small parallaxes ($\varpi < 0.2$ mas), the 5σ interval still overlaps with the $[2.2 - 2.8]$ kpc Carina Nebula distance range for all stars. Therefore, none of our target stars can be reliably classified as background stars based on their Gaia parallaxes. We note that it is very likely that some of our target stars actually are in the background (e.g., as red giants), but the accuracy of the current Gaia parallaxes is just not (yet) good enough to prove this directly from their parallaxes.

6. Properties of the OB2 stars

Since the Gaia data cannot reliably discern stars in TR 16-SE from objects in the galactic background, we need an alternative way to identify possible background stars in our OB2 sample. We therefore calculated the extinction, the absolute K -band magnitude, and, from this, the bolometric magnitude for an assumed distance of 2.3 kpc. The corresponding luminosity estimate is then compared to the expected luminosity of main-sequence stars of this spectral type; if both values agree within a factor of two, we assume the observed stellar properties to be consistent with membership in the Carina Nebula.

We determined the extinction from the $H - K_s$ color excess. For the O-type stars, we assumed the intrinsic colors listed in (Martins et al. 2005) and then used the bolometric corrections

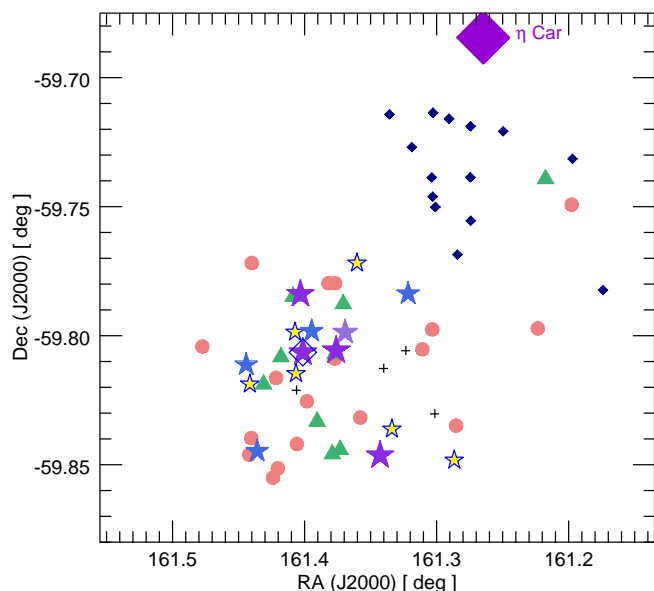


Fig. 2. Map showing the spatial distribution of our KMOS target stars in celestial coordinates. O-type stars are denoted by violet star symbols, early B-type stars with light blue star symbols, (Ae)Be stars with green triangles, and late-type stars with light red circles. The previously known O-type star MJ 596 near the center of the cluster is denoted by an empty diamond (superimposed onto the star symbol). The OB2 stars that we classified as background stars are shown with yellow-filled star symbols. Stars that could not be classified are shown as small crosses, and the OB calibrator stars in Tr 16 are shown with small dark blue diamonds. The position of η Car at the top edge of the map is also indicated.

BC_K from Martins & Plez (2006) to calculate absolute magnitudes and luminosities for $D = 2.3$ kpc. For the early B-type stars, we used the intrinsic colors and bolometric corrections from Pecaut & Mamajek (2013). The calculated luminosities $L[2.3 \text{ kpc}]$ were then compared to the luminosities listed for the corresponding spectral types in Smith (2006).

We found K -band extinction values between 0.64 mag and 1.60 mag, corresponding to visual extinction values of $A_V \sim [5.8 - 14.5]$ mag for the O-type stars in Tr 16-SE. For the O-type stars in Tr 16, which we observed as spectral calibrators, a similar analysis yielded K -band extinction values between 0.24 mag and 0.44 mag, corresponding to visual extinctions of $A_V \sim [2.2 - 4]$ mag.

For nine of the 15 OB2 stars in Tr 16-SE, our luminosity estimates are consistent with their being stars in the Carina Nebula complex, and these stars are thus denoted as "Tr 16-SE members" in Table 4. However, for three O-type stars and three early B-type stars, the computed bolometric luminosity for $D = 2.3$ kpc is more than a factor of 2.5 lower than the expected luminosity for main-sequence stars of this spectral type; these are denoted as "background stars" in Table 4.

7. The stellar population of Tr 16-SE

In Fig. 2 we show the spatial distribution and spectral classifications of our KMOS target stars. We find a clear concentration of OB2 cluster members near the center of the cluster, which is located roughly at the position of the O5 star MJ 596.

In Fig. 3 we show the NIR color-color diagram of the KMOS target stars. It shows that all OB2 stars show extinction values of more than $A_V \geq 5$ mag, clearly suggesting them to

Table 4. Properties of the OB2 stars in the Tr 16-SE region.

Star Name / Position J2000	Spectrum	Spectral Type	A_V [mag]	$\log(L_{\text{bol}}/L_{\odot})$ for $D = 2.3$ kpc	$\log(L_{\text{bol}}/L_{\odot})$ expected	Membership	Comment
J10453631–5948233	B13	O5	6.4	5.33	5.49	Tr 16-SE member	MJ 596
J10453674–5947020	B14	O5	10.3	5.57	5.49	Tr 16-SE member	
J10453024–5948206	B8	O5–6	11.8	5.50	5.32–5.49	Tr 16-SE member	
J10452227–5950470	B5	O6	6.4	5.58	5.32	Tr 16-SE member	MJ 568
J10452862–5947553	B7+C24	O6–7	14.5	5.21	5.14–5.32	Tr 16-SE member	
J10453470–5947537	B12	O9–B1	13.3	4.76	4.37–4.77	Tr 16-SE member	
J10454460–5950411	B18	O9–B1	5.4	4.75	4.37–4.77	Tr 16-SE member	
J10454661–5948404	B21	O9–B1	7.7	4.25	4.37–4.77	Tr 16-SE member	
J10451717–5947013	F7+C20	O9–B1	8.8	4.27	4.37–4.77	Tr 16-SE member	
J10450879–5950537	F3	O6–7	10.5	4.27	5.14–5.23	Background star	
J10452013–5950104	F8	O8–9	7.4	3.91	4.77–4.96	Background star	
J10454595–5949075	F22	O9–B1	5.8	3.83	4.37–4.77	Background star	
J10453755–5948529	F16	B0–1	5.5	3.59	4.37–4.57	Background star	
J10453774–5947552	F17	B0–1	9.1	3.86	4.37–4.57	Background star	
J10452648–5946188	F9+C23	B1–2	7.2	3.84	4.19–4.37	Background star	

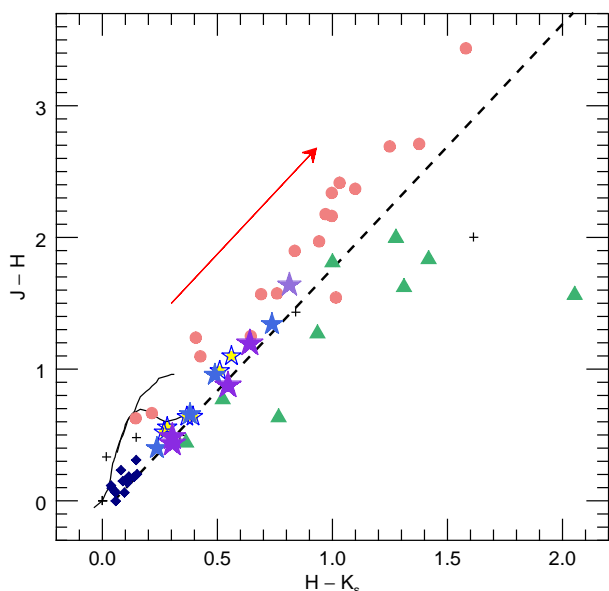


Fig. 3. Near-infrared color-color diagram of the KMOS target stars. The solid lines show the color of the main-sequence and giant stars, the arrow shows an $A_V = 10$ mag reddening vector with slope 1.85 (see Zeidler et al. 2016), and the thick dashed line marks the separation between the photospheric reddening band (above this line) and the infrared excess region (below this line). Symbols and colors for the stars are the same as in Fig. 2.

be located in or (more likely) behind the clouds that obscure Tr 16-SE, as expected. While none of the OB2 stars show evidence for an infrared excess, we note that many (Ae)Be stars do clearly show infrared excesses, as expected for such young stellar objects. Most of the cool stars show high extinction values ($A_V \geq 10$ mag), as expected for background objects that are seen through the clouds obscuring Tr 16-SE.

In Fig. 4 we show an NIR color-magnitude diagram of the KMOS target stars. The locations of the different groups in this diagram are consistent with their spectral classification, which also suggests that a large fraction of the cool stars in our KMOS sample must be red giant stars in the galactic background.

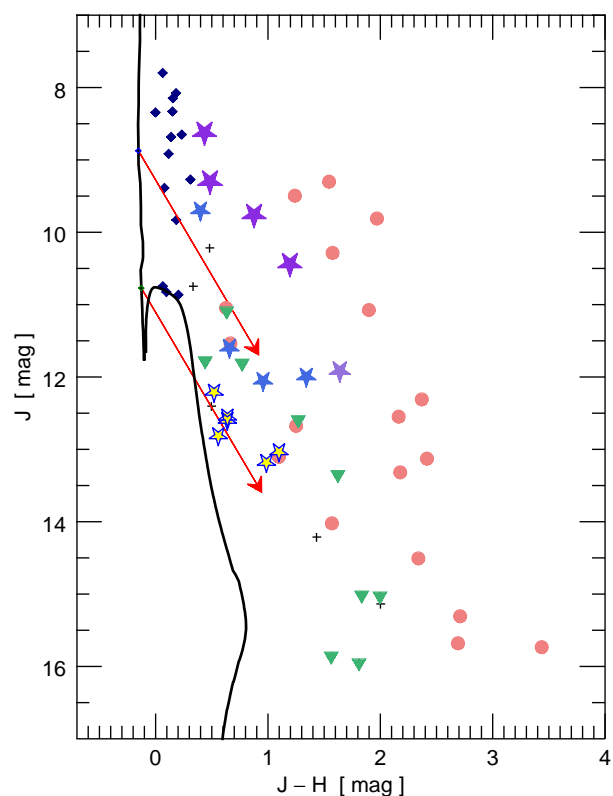


Fig. 4. J versus $J - H$ color-magnitude diagram of the KMOS target stars. The solid black line shows a 1 Myr isochrone based on the PARSEC stellar models (see Bressan et al. 2012). The arrows indicate reddening vectors for $A_V = 10$ mag starting at the location of 10 Myr old stars with masses of $20 M_{\odot}$ and $8 M_{\odot}$. Symbols and colors for the stars are the same as in Fig. 2.

8. Tr 16-SE and the pillar G 287.75–0.66

The *Spitzer* image in Fig. 5 shows the spatial relation between the pillar G 287.75–0.66 and the stars in Tr 16-SE. It shows a bright infrared source located directly at the tip of the pillar. Optical images also show a bright ($V = 13.14$) star (MJ 633) at the pillar tip. This star may thus appear as the “prime suspect” for the radiation source creating and shaping the pillar.

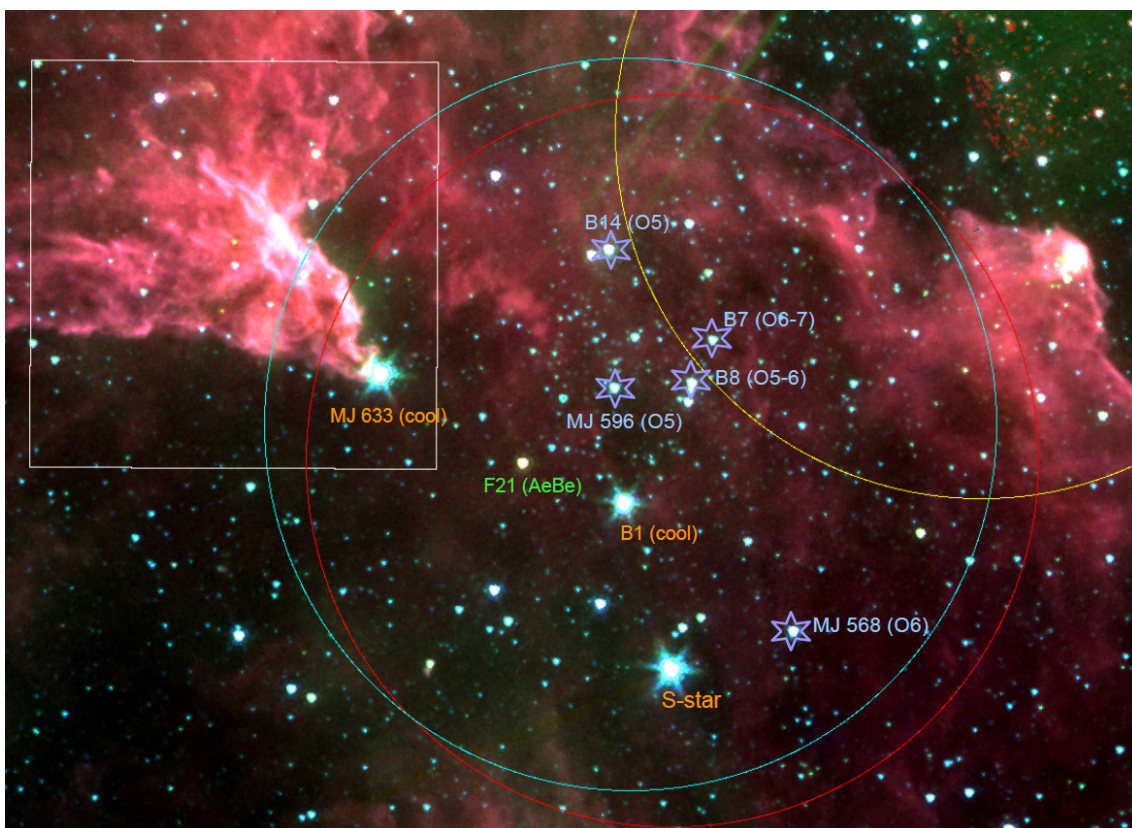


Fig. 5. *Spitzer* Infrared Array Camera (IRAC) color-composite image of Tr 16-SE and the pillar G 287.75–0.66; the image is composed of the $3.6\mu\text{m}$ image in the blue color channel, the $4.2\mu\text{m}$ image in the green color channel, and the $5.8\mu\text{m}$ image in the red color channel. North is up, and east is to the left. The white $4' \times 4'$ square marks the region of the pillar G 287.75–0.66, and the circles show the KMOS patrol fields for the **B** (blue), **F** (red), and **C** (yellow) observations. North is up, and east is to the left. The early O-type stars in Tr 16-SE are marked by the empty violet star symbols; their names and spectral types are given in the annotation. Furthermore, some of the brightest infrared sources (including the S-type star 2MASS J10453185-5951094) are annotated.

However, a detailed inspection of optical⁶ and infrared⁷ images with subarcsecond angular resolution clearly shows that the bright infrared source does not coincide with the optical star MJ 633: There are two distinct sources with an angular separation of $1.8''$. The star MJ 633 is seen as a bright object in the optical image and as a moderately bright object in the NIR image at a consistent position of $\alpha(\text{J2000}) = 10^{\text{h}} 45^{\text{m}} 54.807^{\text{s}}$, $\delta(\text{J2000}) = -59^{\circ} 48' 15.56''$.

The position of the bright infrared source measured in our HAWK-I image is $\alpha(\text{J2000}) = 10^{\text{h}} 45^{\text{m}} 54.575^{\text{s}}$, $\delta(\text{J2000}) = -59^{\circ} 48' 15.1''$; it can be identified with the 2MASS point source J10455458-5948150. This object is also a bright mid-infrared source detected by Mottram et al. (2007) and classified as a massive young stellar object candidate with the designation G 287.7441–00.6869 1. In the optical image, the infrared source is seen as a very faint brightness enhancement in the wings of the PSF of the (optically) much brighter star MJ 633.

In our KMOS observations we obtained spectra of both stars. Our KMOS spectra of the optically visible star MJ 633 (= target F24) show no He I or He II lines, but do show clear CO band head

⁶ We used a 25 sec exposure *r*-SDSS-band image obtained with the ESO VLT Survey Telescope (file name OMEGA.2012-02-15T05:34:43.880.fits) that was obtained as part of the *VST Photometric H- α Survey of the Southern Galactic Plane* (see Drew et al. 2014); it has an image scale of $0.21''$ per pixel and the FWHM of the PSF is $\approx 0.8''$.

⁷ We used our 720 sec exposure *J*-band image obtained with HAWK-I at the ESO VLT (see Preibisch et al. 2011b), which provides an angular resolution of $\approx 0.5''$.

absorption as well as Na and Ca absorption lines. This clearly suggests that MJ 633 is a cool star. Furthermore, the Gaia EDR3 parallax of $\varpi = 0.7480 \pm 0.0127$ mag corresponds to a distance of $D = 1.337$ [1.314 – 1.360] kpc and shows that this star is a foreground object, unrelated to the Carina Nebula. It is just a random projection effect that puts this star apparently at the tip of the pillar.

Our KMOS spectra of the optically invisible infrared-bright star J10455458-5948150 (i.e., target B24) also show no clear signs of He I or He II lines, but do show CO band head absorption as well as Na and Ca absorption, clearly suggesting a cool photosphere. We conclude that the previous classification of this source as a massive young stellar object candidate by Mottram et al. (2007) is not confirmed by our spectra. However, since our spectrum shows the Brackett γ line to be in emission, the object may well be a young stellar object, though not a massive one.

In conclusion, the two stars seen apparently at the tip of the pillar are either unrelated to the Carina Nebula or are not luminous enough to be responsible for producing the pillar. The visual impression that one of these stars is the irradiating source of the pillar is purely a random projection effect.

In Fig. 5 we mark and annotate the early O-type stars in Tr 16-SE; as the emitted stellar UV luminosity is steeply increasing with effective temperature, we only consider the five stars in Tr 16-SE with spectral types between O5 and O6. These five O5-O6 stars are located at projected distances between ≈ 1.7 pc and ≈ 3.1 pc from the pillar; their combined UV irradiation may have shaped the pillar G 287.75–0.66.

9. Conclusions and summary

Our KMOS observations of a magnitude-limited sample of possible OB stars in the obscured cluster Tr 16-SE led to the identification of five stars with spectral types between O5 and O7 (only two of which were known before) and four new stars with spectral types between O9 and B1 as members of Tr 16-SE. With at least five O-type stars and a further four late O- or early B-type stars, Tr 16-SE is one of the larger clusterings of high-mass stars in the Carina Nebula; its high-mass stellar population is smaller than the prominent open clusters Tr 14, 15, and 16 (each of which contains ≥ 15 OB2 stars) but is comparable to or larger than the clusters Bochum 10 (15 OB2 stars) and Bochum 11 (seven OB2 stars). Tr 16-SE therefore constitutes a significant, but so far overlooked, part of the massive cluster population in the Carina Nebula complex.

Our newly identified O-type stars in Tr 16-SE significantly increase the census of spectroscopically identified O-type stars in the Carina Nebula (previously 70 stars). Another very important result is the fact that all six of the OB candidates in Tr 16-SE from Povich et al. (2011) are spectroscopically confirmed as OB2 stars by our KMOS observations. This suggests that the large majority of their 94 OB candidates in the full area of the Carina Nebula are most likely true OB2 stars.

Assuming a $\approx 75\%$ completeness for the Povich et al. (2011) OB-candidate sample (see Sect. 4), this suggests that the Carina Nebula probably contains $\approx (94 - 6)/0.75 \approx 117$ further OB2 stars awaiting spectroscopic confirmation. The total OB2 star population in the Carina Nebula may well be twice as large as the presently identified sample.

Acknowledgements. We thank Rolf Kudritzki and Joachim Puls for enlightening discussion about the spectra of massive stars. The LMU Bachelor Physics student D. Beckord provided assistance in the construction of the initial spectral line catalog. The research of T.P. and B.E. was partly supported by the Excellence Cluster ORIGINS which is funded by the Deutsche Forschungsgemeinschaft (DFG, German Research Foundation) under Germany's Excellence Strategy - EXC-2094 - 390783311. This work has made use of data from the European Space Agency (ESA) mission *Gaia* (<https://www.cosmos.esa.int/gaia>), processed by the *Gaia* Data Processing and Analysis Consortium (DPAC, <https://www.cosmos.esa.int/web/gaia/dpac/consortium>). Funding for the DPAC has been provided by national institutions, in particular the institutions participating in the *Gaia* Multilateral Agreement.

References

Alexander, M. J., Hanes, R. J., Povich, M. S., & McSwain, M. V. 2016, *AJ*, 152, 190
 Bressan, A., Marigo, P., Girardi, L., et al. 2012, *MNRAS*, 427, 127
 Broos, P. S., Getman, K. V., Povich, M. S., et al. 2011, *ApJS*, 194, 4
 Buzzoni, A., Patelli, L., Bellazzini, M., Pecci, F. F., & Oliva, E. 2010, *MNRAS*, 403, 1592
 Coccatto, L., Freudling, W., Smette, A., et al. 2019, *The Messenger*, 177, 14
 Dale, J. E., Ercolano, B., & Bonnell, I. A. 2013, *MNRAS*, 430, 234
 Damiani, F., Kluttsch, A., Jeffries, R. D., et al. 2017, *A&A*, 603, A81
 Davies, B., Kudritzki, R.-P., Plez, B., et al. 2013a, *ApJ*, 767, 3
 Davies, R. I., Agudo Berbel, A., Wiezorrek, E., et al. 2013b, *A&A*, 558, A56
 Drew, J. E., Gonzalez-Solares, E., Greimel, R., et al. 2014, *MNRAS*, 440, 2036
 Feigelson, E. D., Getman, K. V., Townsley, L. K., et al. 2011, *ApJS*, 194, 9
 Freudling, W., Romaniello, M., Bramich, D. M., et al. 2013, *A&A*, 559, A96
 Gaia Collaboration, Brown, A. G. A., Vallenari, A., et al. 2020, *arXiv e-prints*, arXiv:2012.01533
 Gaia Collaboration, Prusti, T., de Bruijne, J. H. J., et al. 2016, *A&A*, 595, A1
 Gray, R. O. & Corbally, Christopher, J. 2009, *Stellar Spectral Classification*, Princeton Series in Astrophysics (Princeton University Press)
 Gritschneider, M., Burkert, A., Naab, T., & Walch, S. 2010, *ApJ*, 723, 971
 Hanes, R. J., McSwain, M. V., & Povich, M. S. 2018, *AJ*, 155, 190
 Hanson, M. M., Kudritzki, R.-P., Kenworthy, M. A., Puls, J., & Tokunaga, A. T. 2005, *ApJS*, 161, 154
 Herbig, G. H. 1994, in *Astronomical Society of the Pacific Conference Series*, Vol. 62, *The Nature and Evolutionary Status of Herbig Ae/Be Stars*, ed. P. S. The, M. R. Perez, & E. P. J. van den Heuvel, 3

Kiminki, M. M. & Smith, N. 2018, *MNRAS*, 477, 2068
 Klaassen, P. D., Reiter, M. R., McLeod, A. F., et al. 2020, *MNRAS*, 491, 178
 Martins, F. & Plez, B. 2006, *A&A*, 457, 637
 Martins, F., Schaerer, D., & Hillier, D. J. 2005, *A&A*, 436, 1049
 Massey, P. & Johnson, J. 1993, *AJ*, 105, 980
 McLeod, A. F., Gritschneider, M., Dale, J. E., et al. 2016, *MNRAS*, 462, 3537
 Mohr-Smith, M., Drew, J. E., Napiwotzki, R., et al. 2017, *MNRAS*, 465, 1807
 Mottram, J. C., Hoare, M. G., Lumsden, S. L., et al. 2007, *A&A*, 476, 1019
 Niemela, V. S., Morrell, N. I., Fernández Lajús, E., et al. 2006, *MNRAS*, 367, 1450
 Pecaut, M. J. & Mamajek, E. E. 2013, *ApJS*, 208, 9
 Povich, M. S., Maldonado, J. T., Haze Nuñez, E., & Robitaille, T. P. 2019, *ApJ*, 881, 37
 Povich, M. S., Townsley, L. K., Broos, P. S., et al. 2011, *ApJS*, 194, 6
 Preibisch, T., Fleischlen, S., Gaczkowski, B., Townsley, L., & Broos, P. 2017, *A&A*, 605, A85
 Preibisch, T., Hodgkin, S., Irwin, M., et al. 2011a, *ApJS*, 194, 10
 Preibisch, T., Ratzka, T., Kuderna, B., et al. 2011b, *A&A*, 530, A34
 Preibisch, T., Roccatagliata, V., Gaczkowski, B., & Ratzka, T. 2012, *A&A*, 541, A132
 Preibisch, T., Schuller, F., Ohlendorf, H., et al. 2011c, *A&A*, 525, A92
 Preibisch, T., Zeidler, P., Ratzka, T., Roccatagliata, V., & Petr-Gotzens, M. G. 2014, *A&A*, 572, A116
 Rebolledo, D., Burton, M., Green, A., et al. 2016, *MNRAS*, 456, 2406
 Repolust, T., Puls, J., Hanson, M. M., Kudritzki, R. P., & Mokiem, M. R. 2005, *A&A*, 440, 261
 Roccatagliata, V., Preibisch, T., Ratzka, T., & Gaczkowski, B. 2013, *A&A*, 554, A6
 Sanchawala, K., Chen, W.-P., Lee, H.-T., et al. 2007, *ApJ*, 656, 462
 Sharples, R., Bender, R., Agudo Berbel, A., et al. 2013, *The Messenger*, 151, 21
 Smith, N. 2006, *MNRAS*, 367, 763
 Smith, N. & Brooks, K. J. 2008, *ASP Monograph Publications*, Vol. 5, *The Carina Nebula: A Laboratory for Feedback and Triggered Star Formation*, ed. B. Reipurth (Astronomical Society of the Pacific), 138
 Smith, N., Povich, M. S., Whitney, B. A., et al. 2010, *MNRAS*, 406, 952
 Sota, A., Maíz Apellániz, J., Morrell, N. I., et al. 2014, *ApJS*, 211, 10
 Stoehr, F., White, R., Smith, M., et al. 2008, *ASP Conference Series*, Vol. 394, *DER_SNR: A Simple & General Spectroscopic Signal-to-Noise Measurement Algorithm*, ed. R. W. Argyle, P. S. Bunclark, & J. R. Lewis (Astronomical Society of the Pacific), 505
 Townsley, L. K., Broos, P. S., Corcoran, M. F., et al. 2011, *ApJS*, 194, 1
 Van Eck, S., Jorissen, A., Udry, S., et al. 2000, *A&AS*, 145, 51
 Zeidler, P., Preibisch, T., Ratzka, T., Roccatagliata, V., & Petr-Gotzens, M. G. 2016, *A&A*, 585, A49

Appendix A: Spectra

Figures A.1 to A.6 show the normalized KMOS spectra of all our targets.

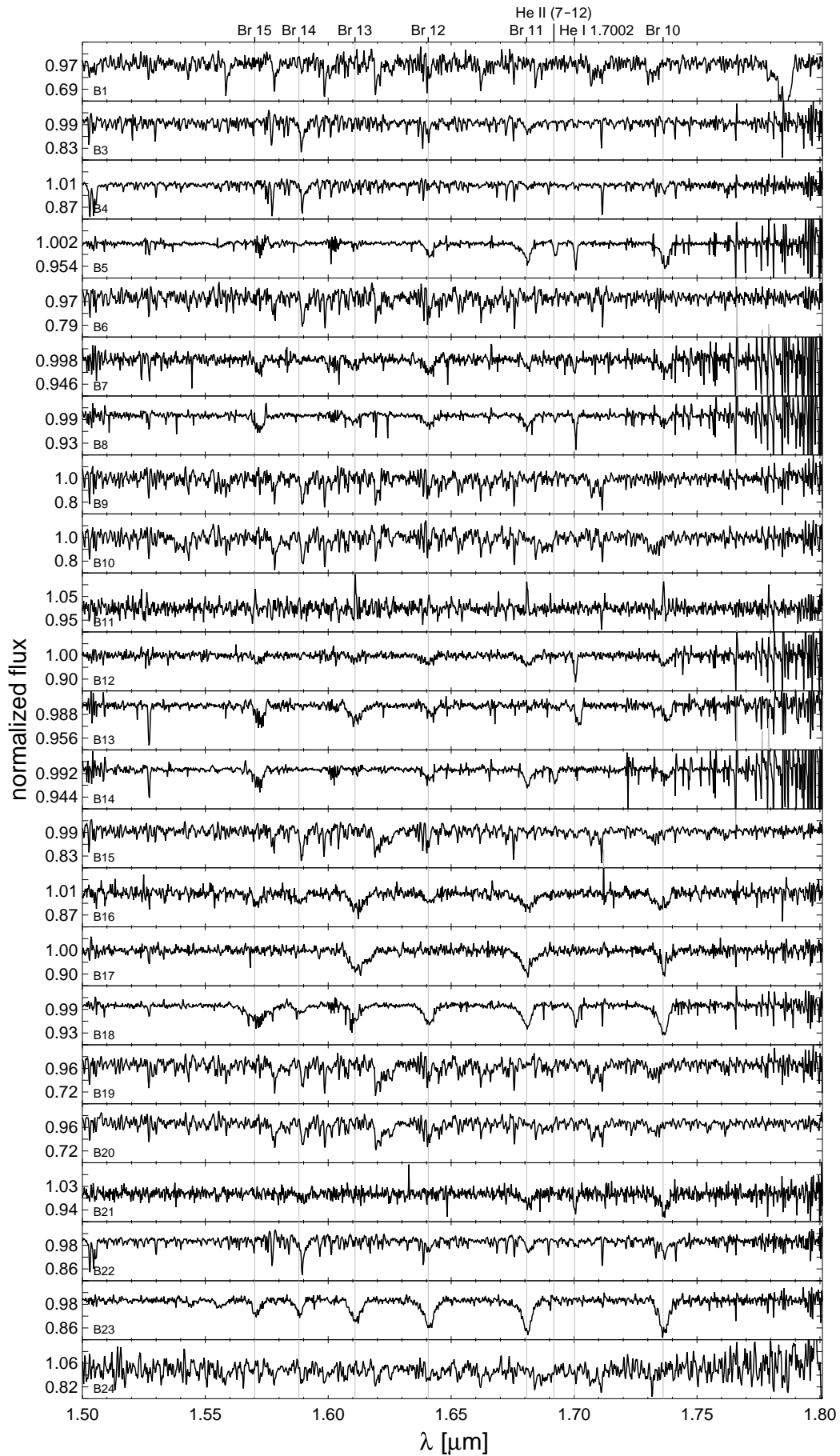


Fig. A.1. *H*-band spectra in the **B** sample.

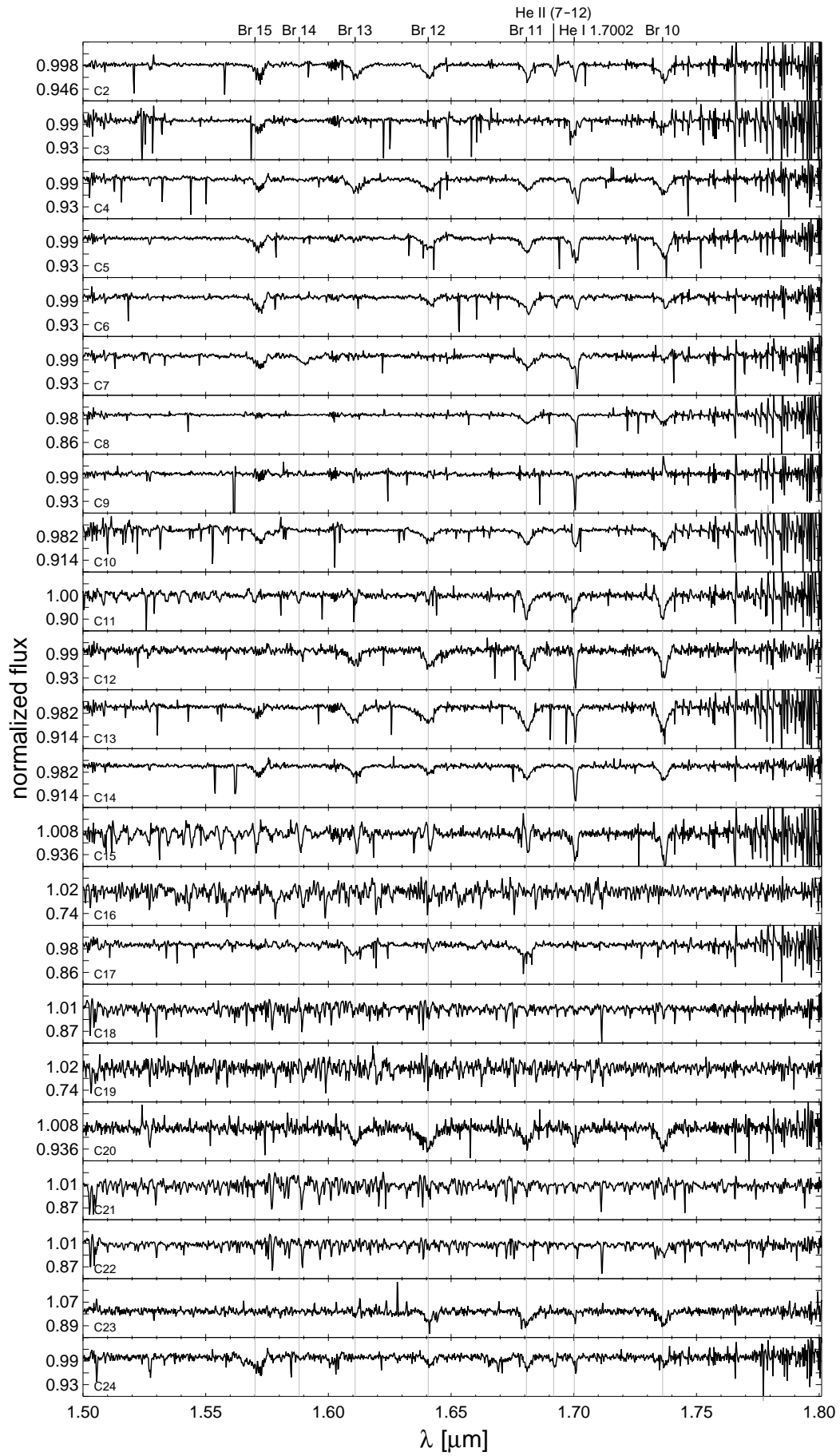


Fig. A.2. *H*-band spectra in the C sample.

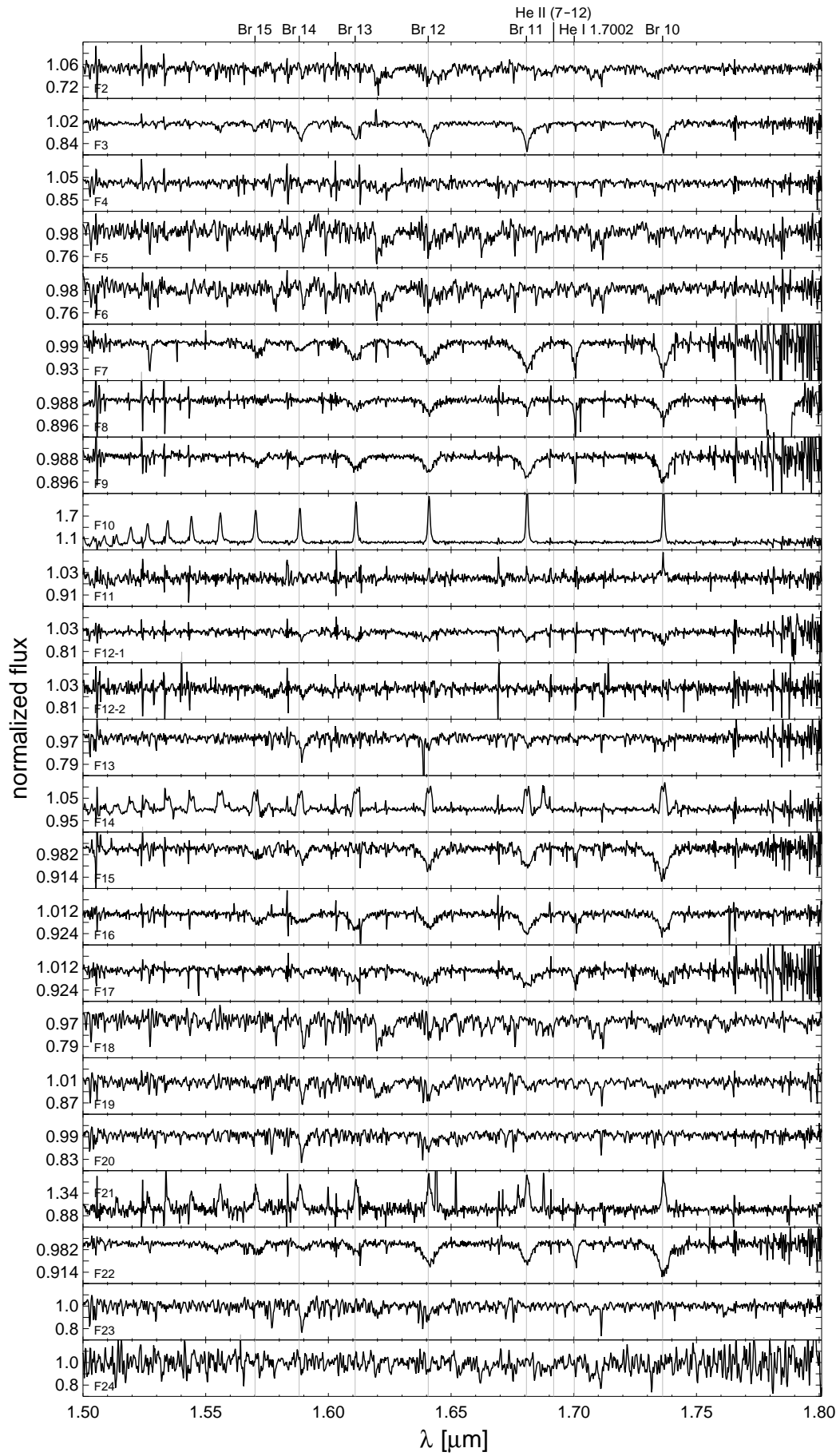


Fig. A.3. *H*-band spectra in the **F** sample.

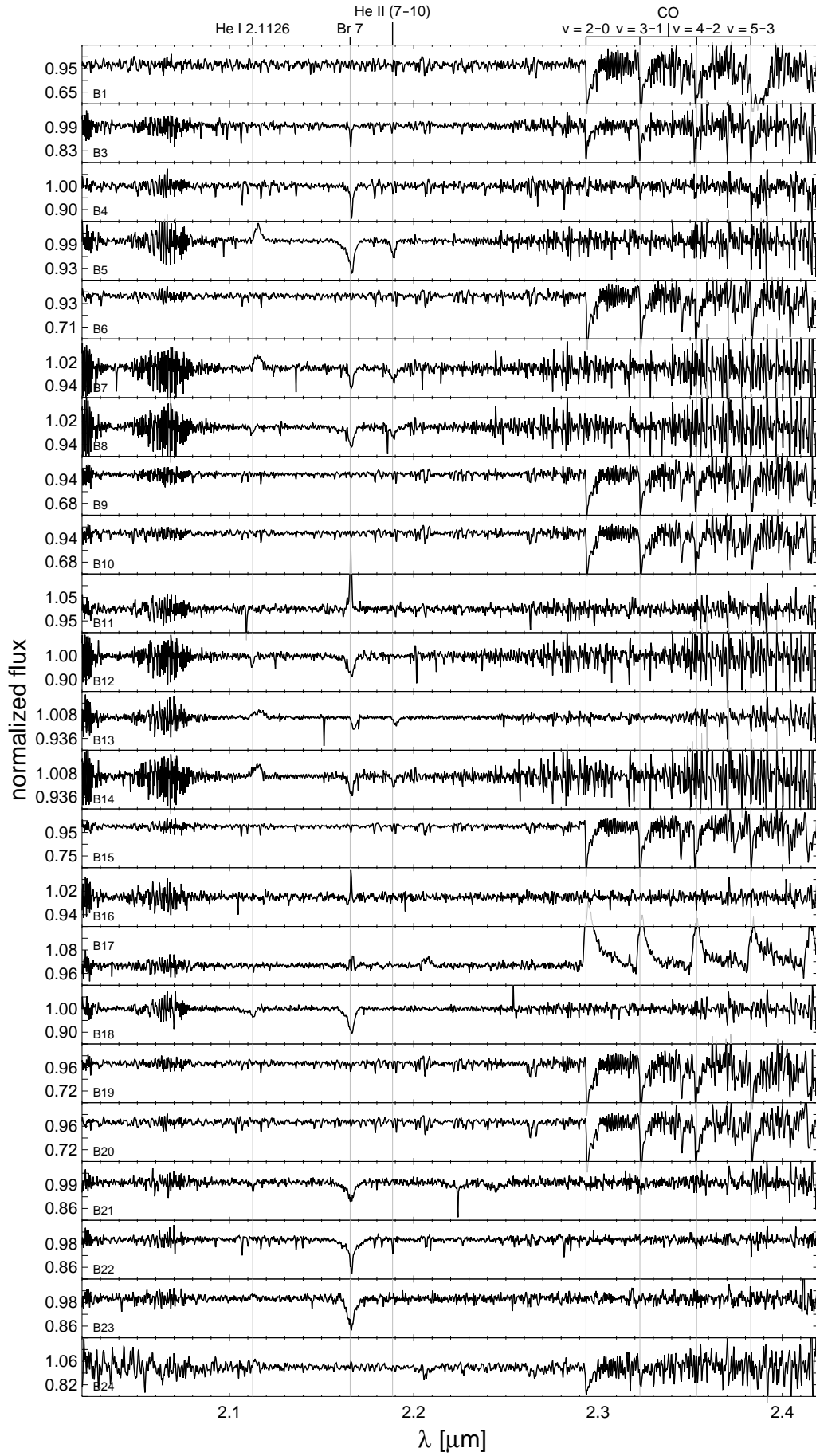


Fig. A.4. K-band spectra in the B sample.

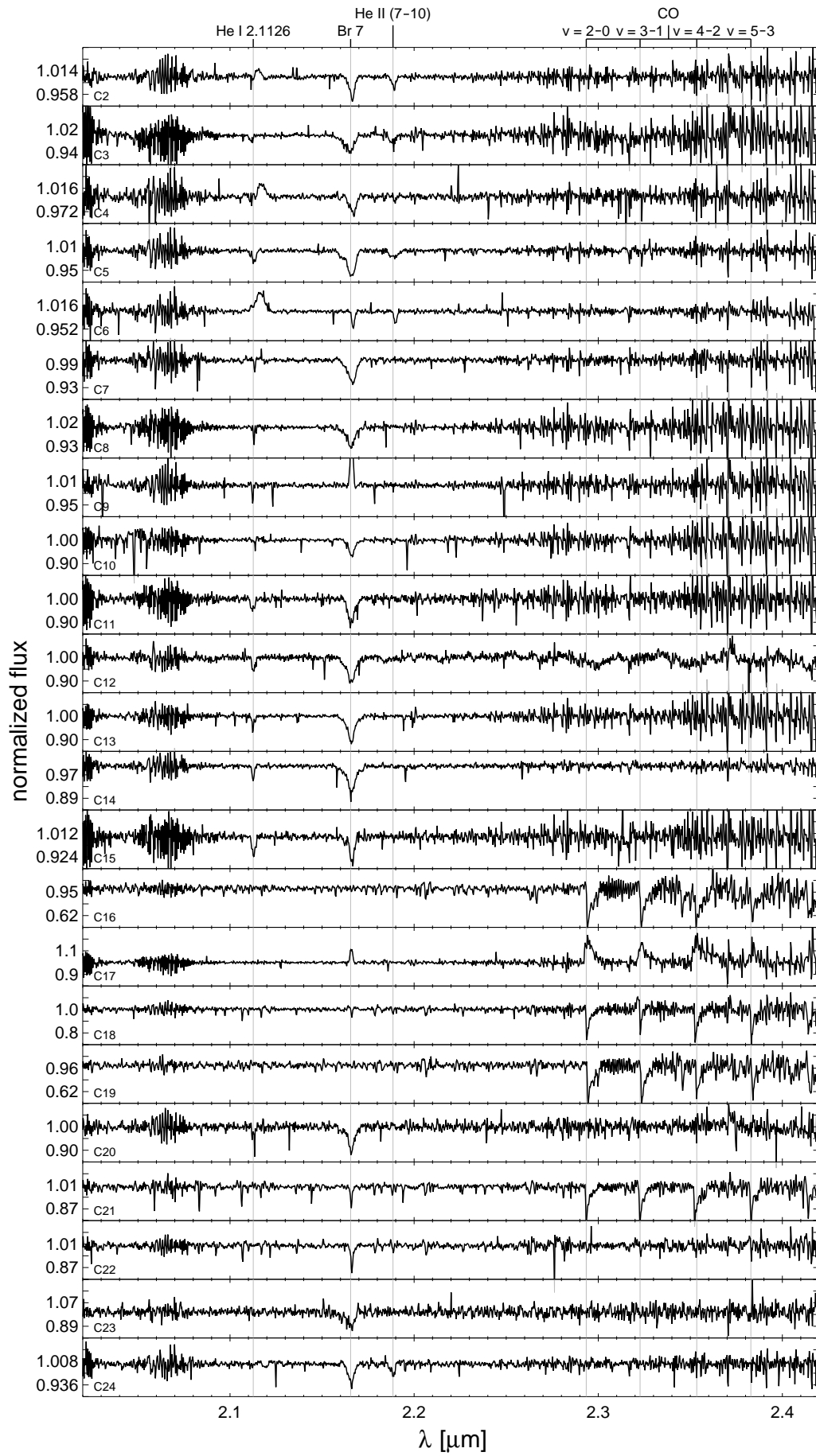


Fig. A.5. *K*-band spectra in the C sample.

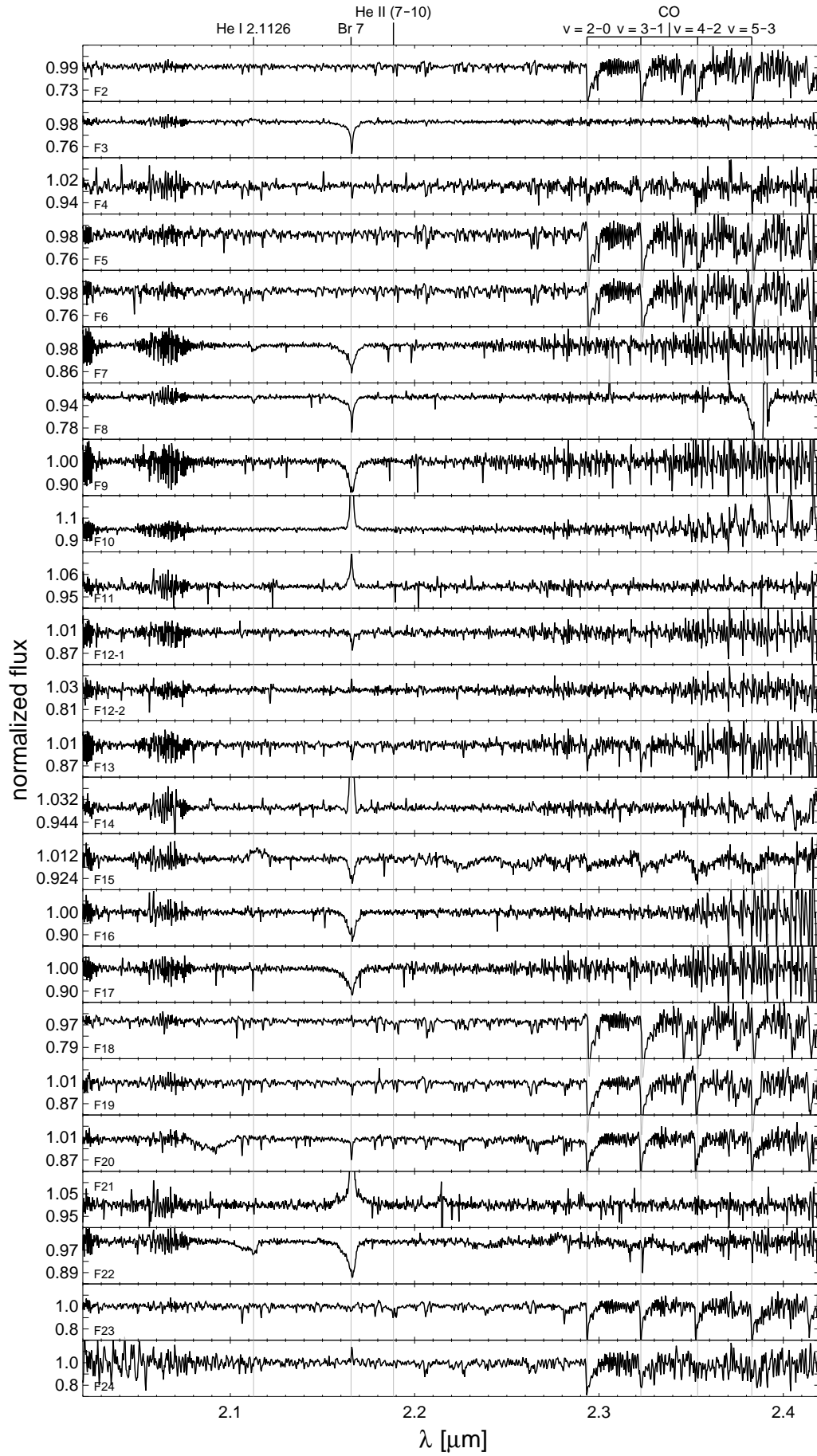


Fig. A.6. K-band spectra in the F sample.

Table 3. Target positions and results.

Star name / position [J2000]	Spectrum	opt. mag	<i>J</i> [mag]	<i>H</i> [mag]	<i>K_s</i> [mag]	CCCP Match	Spectral Type	Comment
2MASS J10444745-5944572	C16	<i>G</i> = 16.01	10.28	8.71	7.95	...	cool	in Tr 16
2MASS J10445220-5944212	C17	<i>G</i> = 12.48	11.09	10.45	9.69	...	(Ae)Be	in Tr 16; CO emission
2MASS J10445360-5947498	C18	<i>G</i> = 14.42	11.05	10.42	10.27	...	cool	in Tr 16, foreground star
2MASS J10450845-5950054	F2	...	15.73	12.30	10.72	...	cool	
2MASS J10450879-5950537	F3	<i>G</i> = 17.24	13.03	11.93	11.37	...	O6-7	
2MASS J10451232-5949490	F4	<i>G</i> = 18.90	15.14	13.14	11.52	...	≥ B2	
2MASS J10451278-5947511	F5 + C19	...	15.31	12.60	11.22	...	cool	
2MASS J10451459-5948190	F6	...	15.68	12.99	11.74	...	cool	
2MASS J10451717-5947013	F7 + C20	<i>G</i> = 16.02	12.05	11.10	10.61	104517.21-594701.6	O9-B1	OBe 48
2MASS J10451758-5948209	B3 + C21	<i>G</i> = 11.82	10.22	9.74	9.59	...	cool	foreground star
2MASS J10452013-5950104	F8	<i>G</i> = 15.49	12.60	11.96	11.59	...	O8-9	
2MASS J10452160-5948457	B4 + C22	<i>G</i> = 11.91	10.75	10.41	10.40	...	AFG?	foreground star
2MASS J10452227-5950470	B5	<i>G</i> = 10.77	8.62	8.19	7.88	104522.29-595047.0	O6	MJ 568, OBc 50
2MASS J10452586-5949540	B6	<i>G</i> = 19.61	13.32	11.14	10.17	...	cool	
2MASS J10452648-5946188	F9 + C23	<i>G</i> = 15.50	12.55	11.91	11.52	...	B1-2	
2MASS J10452862-5947553	B7 + C24	<i>G</i> = 17.50	11.91	10.28	9.46	104528.60-594756.1	O6-7	OBe 51
2MASS J10452898-5947157	F10	<i>i</i> = 20.26	15.03	13.03	11.75	...	Be	
2MASS J10452952-5950390	F11	<i>G</i> = 18.88	15.01	13.18	11.76	...	(Ae)Be	
2MASS J10453024-5948206	B8	<i>G</i> = 15.32	10.43	9.24	8.60	104530.22-594821.0	O5-6	OBe 52
VCNS J104530.29-594824.5	F12-1	<i>G</i> = 19.67	14.21	12.78	11.94	...	B?	
HAWK-I J104530.42-594825.4	F12-2	<i>i</i> = 20.68	15.95	14.14	13.14	...	(Ae)Be	
2MASS J10453045-5946467	B9	<i>G</i> = 19.89	13.13	10.71	9.68	...	cool	
2MASS J10453053-5948317	B10	<i>G</i> = 19.16	12.55	10.39	9.39	...	cool	
2MASS J10453095-5950451	B11	<i>G</i> = 16.12	12.59	11.32	10.39	104530.96-595045.4	(Ae)Be	
2MASS J10453166-5946467	F13	<i>G</i> = 19.21	14.02	12.45	11.76	...	cool(?)	
2MASS J10453372-5949596	F14	<i>G</i> = 14.20	11.78	11.34	10.97	104533.73-595000.5	(Ae)Be	
2MASS J10453470-5947537	B12	<i>G</i> = 17.18	11.99	10.65	9.91	...	O9-B1	
2MASS J10453556-5949314	B1	<i>G</i> = 16.08	9.81	7.84	6.90	104535.76-594932.7	cool	
2MASS J10453631-5948233	B13	<i>G</i> = 11.71	9.29	8.81	8.51	104536.33-594823.5	O5	MJ 596 = V662 Car
2MASS J10453674-5947020	B14	<i>G</i> = 13.59	9.76	8.88	8.33	104536.75-594702.2	O5	OBe 56
2MASS J10453739-5950310	B15	<i>G</i> = 13.06	9.49	8.26	7.85	...	cool	
2MASS J10453745-5949161	F15	<i>G</i> = 14.68	12.40	11.91	11.57	104537.48-594916.5	Be?	He I emission + CO absorption
2MASS J10453755-5948529	F16	<i>G</i> = 15.41	12.81	12.25	11.97	...	B0-1	
2MASS J10453774-5947552	F17	<i>G</i> = 17.22	13.18	12.19	11.68	...	B0-1	
2MASS J10453806-5947052	B16	<i>G</i> = 18.24	13.35	11.73	10.41	...	(Ae)Be	
2MASS J10454029-5948297	B17	<i>G</i> = 15.16	11.81	11.04	10.52	104540.44-594830.6	(Ae)Be	CO emission
2MASS J10454085-5951048	F18	<i>i</i> = 20.62	14.51	12.17	11.17	...	cool	
2MASS J10454118-5948587	F19	<i>G</i> = 16.04	12.68	11.42	10.78	...	cool	
2MASS J10454173-5951180	F20	<i>G</i> = 16.92	13.10	12.01	11.58	...	cool	
2MASS J10454344-5949075	F21	<i>G</i> = 19.38	15.86	14.29	12.24	...	(Ae)Be	
2MASS J10454460-5950411	B18	<i>G</i> = 11.85	9.70	9.30	9.06	...	O9-B1	
2MASS J10454559-5946184	B19	<i>G</i> = 19.23	12.31	9.94	8.84	...	cool	
2MASS J10454569-5950227	B20	<i>G</i> = 16.96	11.07	9.18	8.34	...	cool	
2MASS J10454595-5949075	F22	<i>G</i> = 14.82	12.21	11.69	11.42	...	O9-B1	

Table 3. Continued.

Star name / position [J2000]	Spectrum	opt. mag	J	H	K_s	CCCP Match	Spectral Type	Comment
2MASS J10454606-5950460	F23	$G = 13.82$	11.54	10.87	10.65	...	cool	foreground star
2MASS J10454661-5948404	B21	$G = 14.63$	11.59	10.94	10.56	104546.64-594840.2	O9-B1	OBC 61
2MASS J10454845-5950343	B22	$G = 11.25$	10.18	9.89	9.84	...	B/A?	foreground star
2MASS J10455242-5949073	B23	$G = 11.20$	10.83	10.81	10.78	...	B?	foreground star
2MASS J10455458-5948150	B24	$r = 17.58$	9.30	7.76	6.74	...	cool	= pillar tip star
HAWK-I J104554.77-594815.5	F24	$G = 13.35$	12.38	...	11.66	...	cool	MJ 633, foreground star

Notes. Optical magnitudes are from Gaia EDR3 (G), if available, or are r - or i -band values from the *VST Photometric H- α Survey of the Southern Galactic Plane* (see Drew et al. 2014). Near-infrared magnitudes are from our *VISTA Carina Nebula Survey* (Preibisch et al. 2014) and HAWK-I (Preibisch et al. 2011b). X-ray source matches refer to the source catalog of the *CCCP* (Townsend et al. 2011).